THE EFFECT OF VARYING SECONDARY STAGNATION TEMPERATURE AND MOLECULAR WEIGHT ON THE SIDE FORCE GENERATED BY GASEOUS INJECTION INTO A SUPERSONIC STREAM

by

Russel Allen Chambers

United States
Naval Postgraduate School

THESIS

THE EFFECT OF VARYING SECONDARY STAGNATION TEMPERATURE AND MOLECULAR WEIGHT ON THE SIDE FORCE GENERATED BY GASEOUS INJECTION INTO A SUPERSONIC STREAM

by

Russel Allen Chambers

October 1969

The Effect of Varying Secondary Stagnation Temperature and Molecular Weight on the Side Force Generated by Gaseous Injection into a Supersonic Stream

by

Russel Allen Chambers
Captain, United States Marine Corps
B.S., University of Kansas, 1962

Submitted in partial fulfillment of the
requirements for the degree of

MASTER OF SCIENCE IN AERONAUTICAL ENGINEERING

from the

NAVAL POSTGRADUATE SCHOOL
October 1969

ABSTRACT

This study was undertaken to investigate the effects of varying the injectant temperature and molecular weight on the flow field generated by the interaction of a secondary jet with a supersonic mainstream. The experimental portions of this investigation were conducted at a primary Mach number of 1.92 in the Naval Postgraduate School Supersonic Wind Tunnel. Data are presented and compared with theory. This presentation includes correlation of the penetration height of the secondary flow, interaction side force amplification factor, and separation distance non-dimensionalized with respect to the penetration height.

TABLE OF CONTENTS

LIST OF FIGURES

LIST OF SYMBOLS

Symbol	Definition
A	side force amplification factor
A_*	nozzle throat area
c	nozzle discharge coefficient
Cp	pressure coefficient
d	nozzle throat diameter
F_i	interaction side force
F_j	secondary nozzle thrust
h	penetration height of secondary injectant
k_i	constant from evaluation of the blast wave theory pressure distribution function integral
M	Mach number
$\dot{m}_s$	secondary mass flow rate
$\mathcal{m}$	molecular weight
P	pressure
P_{pt}	primary stream total pressure
P_{st}	secondary stream total pressure
q	dynamic pressure
R	gas constant
R_o	blast wave characteristic radius
s	length of plate
T_{pt}	primary stream total temperature
T_{st}	secondary stream total temperature
v	flow velocity
J_o	first order blast wave constant

Symbol	Definition
Δx	boundary layer separation distance
γ	ratio of specific heats
θ	separation angle

Subscripts

∞	free stream
p	primary fluid
s	secondary fluid

ACKNOWLEDGEMENTS

The author would like to express his indebtedness to Professor Daniel J. Collins for his guidance in all phases of this study and a special thanks to Mr. Norman Leckenby and Mr. Bert Funk, Mechanical and Aerospace Engineering Technicians, for making the experimental portions of this investigation an enjoyable experience.

I. INTRODUCTION

Understanding of the interaction between a lateral jet and a supersonic stream is the foundation for the implementation of jet reaction control systems currently being investigated for use in missile control. Recently a number of papers have been published on this subject [Refs. 1, 3, 4, 5, and 9] and each investigation contributes additional understanding of the overall complex problem. This study is intended to further the understanding of how the side force amplification factor is affected by the flow parameters; injection pressure, injection temperature, injection molecular weight and free stream Mach number. The significance of the separation distance and penetration height as a predictor of the amplification factor is also investigated.

Many investigators [Refs. 1, 4, and 9] have been concerned with injecting a gas laterally through a flat plate mounted in a wind tunnel. In the present investigation, however, in order to eliminate flow blockage at low Mach number, the secondary gas was injected directly through the bottom of the tunnel. The boundary layer is, therefore, thicker than those associated with the flat plate.

This investigation was performed in the Naval Postgraduate School supersonic wind tunnel at a Mach number of 1.92 by injecting gaseous nitrogen, helium and argon through a sonic nozzle mounted normal to the tunnel wall. The parameters varied during the experiment include injectant stagnation temperature and pressure, injectant exit area, and injectant gas (molecular weight and specific heat ratio).

II. EXPERIMENTAL SET-UP

The Naval Postgraduate School supersonic wind tunnel is a blow-down model with a 4-inch by 4-inch test section, 6 inches long. The tunnel is capable of approximately 5 minutes of continuous operation. Total pressure and total temperature of the primary flow were measured in the wind tunnel plenum chamber, and remained constant for each experimental run.

The injection equipment used in this thesis was arranged as shown in Fig. 1. Figures 2 and 3 are photographs of the test set-up. Bottles of compressed gaseous injectant were obtained commercially and fed into the system through a pressure regulator. The flow was passed through a sharp-edged orifice flowmeter, into the heater, and onto the sonic nozzle mounted flush with the floor of the tunnel test section.

The heating system was the same system used by Chrans and Collins [Ref. 1] and consisted of coiled steel tubing placed in an insulated container. An arc welder was connected across the ends of the coil and the coil was heated by passing an electric current through the steel tubing. The injectant gas was subsequently heated through contact with the hot tubing.

Stagnation conditions were achieved between the heater and the nozzle by an expansion chamber developed by Chrans and Collins. Stagnation pressure and temperature of the secondary flow were measured at this point. Stagnation temperature was measured by means of a chromel-alumel thermocouple at the expansion chamber.

The two sonic nozzles used were simple converging nozzles with parallel side walls at the exit section as shown in Fig. 4. Exit diameters of 0.1406 inches and 0.075 inches were used during the experiment. The nozzle was fastened to the top of the expansion chamber and then mounted to the bottom of the tunnel.

A special phenolic supersonic tunnel block was fabricated to allow gaseous injection directly through the floor of the tunnel. An aluminum plug was screw-fitted into the phenolic block to accomodate the nozzle and to prevent heat damage to the test section. Forty-seven pressure taps were located on the floor of the tunnel in a pattern shown in Fig. 5. Measurements from these pressure taps were used to obtain interaction side force data.

The pressures were measured at the pressure taps by a Scanivalve calibrated in inches of mercury vacuum. The measurements were recorded on a Honeywell Visicorder.

Schlieren photographs on Polaroid 4x5 type 55 P/N positive-negative film were taken of each run using an offset Schlieren system with collimating mirrors. An optical comparator was used to measure the penetration height and separation distance from the negative film.

III. EXPERIMENTAL PROCEDURE

Although the wind tunnel block was designed to yield Mach 2.0, several experimental tare runs were made with no secondary injection to obtain the actual Mach number in the tunnel test section. The wind tunnel plenum pressure was held constant at 30 psi. Static pressure measurements varied between 4.20 and 4.40 psi. The average static pressure was calculated to be 4.34 psi. Using Table III of Ref. 2 the primary Mach number of the tunnel was determined to be 1.92 ± 0.01.

Figure 6 depicts the run matrix for this thesis, showing the room temperature runs (1-16, 56-71) and the runs at higher temperature. For each run the primary stagnation pressure was held constant at 30 psi while the secondary stagnation pressure was varied from 20 psi to 180 psi, giving a pressure ratio range of from 2/3 to 6. The following observations were made for each run:

1. The static pressure at each of the 47 pressure taps was measured by a Scanivalve and recorded on a Visicorder.
2. The differential pressure through the flowmeter was measured from a mercury manometer.
3. The upstream flowmeter pressure was recorded by a pressure gauge.
4. The injection total pressure was measured by a pressure gauge.
5. The primary total pressure was measured by a pressure gauge.
6. The total temperature of the secondary flow through the flowmeter was sensed, for mass flow measurement, by a chromel-alumel thermocouple and displayed on a portable potentiometer.
7. A Schlieren photograph was taken of the test section.

A second chromel-alumel thermocouple was used to record primary and secondary stagnation temperatures in the following manner. For the

room temperature runs, primary total temperature was sensed by a chromel-alumel thermocouple and displayed on the potentiometer. Secondary total temperature at the nozzle was assumed to be the same as that through the flowmeter. For the high temperature runs, primary total temperature was assumed to be the average of the primary stagnation temperatures (510° R) in Runs 1-16, and total secondary temperature at the nozzle was sensed by a chromel-alumel thermocouple in the expansion chamber and displayed on a potentiometer.

Tare pressures were recorded without secondary injection and subtracted from corresponding pressures measured during injection. The resulting pressures were integrated over the affected area to obtain the interaction side force.

Penetration height and separation distance were measured from the Schlieren photographs with the use of an optical comparator and then scaled to the actual size of the test section.

IV. THEORETICAL BACKGROUND

The investigation of interaction between primary and secondary streams requires extensive experimentation and the analysis of many variables. Penetration height, separation distance, side force and amplification ratio will be treated in this thesis in an attempt to establish correlations that will be useful in understanding interaction phenomena. This investigation is limited to sonic injection of secondary gas normal to the primary stream.

Figure 7 is a sketch of the flow field produced by secondary injection. This sketch is based on examination of Schlieren photographs taken during the experimental runs. Figures 8 and 9 are typical Schlieren photographs. The penetration height h has been considered by most investigators as the characteristic length of the flow field.

Photographs of the interaction phenomena indicate the boundary layer separates some distance ahead of the bow shock induced by secondary flow. This separation distance is important since, as determined by Zukoski and Spaid [Ref. 3] and confirmed by Koch [Ref. 4], the surface area ahead of the injector is subjected to the highest interaction pressures developed during secondary injection.

Side force and the force amplification factor appear to be two of the most important parameters that must be understood by engineers engaged in the design and development of thrust vector control of missiles.

A. PENETRATION HEIGHT

Zukoski and Spaid have suggested a model of interaction flow based on hypersonic flow past a blunt body. Assumptions used in this model are as follows:

1. Sonic injection into a uniform supersonic flow with no boundary layer.
2. No mixing between primary and secondary flow.
3. The blunt body to be a quarter sphere with a semi-cylindrical afterbody.
4. The injectant gas remains within the confines of the blunt body.

By balancing the profile drag of the blunt body against the change in momentum flux of the injectant gas, the radius of the blunt body can be found. Zukoski and Spaid suggest that the magnitude of this radius is representative of the penetration height of the secondary injectant. The relationship developed by Zukoski and Spaid is given by

$$\frac{h}{d\sqrt{C}} = \frac{1}{M_\infty}\left(\frac{P_{ST}}{P_\infty}\,\frac{\gamma_s}{\gamma_\infty}\,\frac{2}{C_p}\right)^{\frac{1}{2}}\left\{\frac{2}{\gamma_s-1}\left(\frac{2}{\gamma_s+1}\right)^{\frac{\gamma_s+1}{\gamma_s-1}}\left[1-\left(\frac{P_\infty}{P_{ST}}\right)^{\frac{\gamma_s-1}{\gamma_s}}\right]\right\}^{\frac{1}{4}} \qquad (1)$$

Chrans and Collins investigated the effect of secondary temperature on the penetration height and detected no essential difference in this dimension as temperature was varied from 500°R to 1500°R and secondary stagnation pressure was held constant. They concluded that either the penetration height is a function of secondary momentum or at most a weak function of secondary total temperature.

Cassel, Davis and Engh [Ref. 5] employed a blunt body analogy of the flow field in a manner similar to the method of Zukoski and Spaid,

and developed an expression for penetration height given by

$$\frac{h}{d\sqrt{c}} = \frac{3}{4}\left[(\gamma_s+1)\left(\frac{2}{\gamma_s+1}\right)^{\frac{\gamma_s}{\gamma_s-1}}\right]^{\frac{1}{2}} \left(\frac{P_{sr}}{q}\right)^{\frac{1}{2}} \qquad (2)$$

where q is the primary dynamic pressure. Values of q may be determined from Ref. 6.

B. SEPARATION DISTANCE

The separation distance, shown in Fig. 7, is defined as the distance from the center of the injection port to the beginning of flow separation due to lateral injection.

A three-dimensional model suggested by Wu, Chapkis and Mager [Ref. 7] assumes the separation shock to be conical and, by the geometry of the model, separation distance is given by

$$\Delta x = h \cot \theta \qquad (3)$$

where θ is the separation shock angle. For this model the separation angle θ is assumed to depend upon mainstream Mach number and the specific heat ratio of the secondary stream. References 6 and 8 give charts and tables allowing determination of the conical shock angle θ for various specific heat ratios and primary stream Mach numbers.

C. SIDE FORCE AND AMPLIFICATION FACTOR

In this study side force data are non-dimensionalized with respect to the jet thrust of the secondary flow to obtain a side force amplification factor.

Zukoski and Spaid state that if Equation (1) can be taken as a good approximation to the penetration height, then the side force generated on an infinite flat plate can be easily calculated as follows:

$$F_i = \int_{x=-\infty}^{\infty} \int_{y=-\infty}^{\infty} (P - P_\infty)\, dy\, dx \tag{4}$$

where F_i is the side force contribution from the pressure field resulting from interaction. Dividing through by $P_\infty h^2$ results in

$$\frac{F_i}{P_\infty h^2} = \int_{\frac{x}{h}=-\infty}^{\infty} \int_{\frac{y}{h}=-\infty}^{\infty} \left(\frac{P - P_\infty}{P_\infty}\right) \frac{dy}{h} \frac{dx}{h} \equiv \Phi \tag{5}$$

Since the integral in Equation (5) is evaluated in normalized coordinates, its value will depend only upon the free stream Mach number and specific heat ratio, that is

$$\Phi = \Phi\{M_\infty, \gamma_\infty\} \tag{6}$$

Equation (5) can now be written

$$F_i = P_\infty \Phi\{M_\infty, \gamma_\infty\} h^2 \tag{7}$$

or for a given set of primary conditions

$$F_i \propto h^2 \tag{8}$$

In further treatment Zukoski and Spaid suggest that for given free stream conditions

$$F_i \propto \dot{m}_s \left(R_s T_{st} \right)^{\frac{1}{2}} \tag{9}$$

They also state that for $P_{st}/P_\infty \gg 1$ the thrust of a sonic jet, F_j , can be written

$$F_j \propto \dot{m}_s \left(R_s T_{st} \right)^{\frac{1}{2}} \tag{10}$$

The total normal force due to injection is then

$$F_i + F_j \propto \dot{m}_s \left(R_s T_{st} \right)^{\frac{1}{2}} \tag{11}$$

If the amplification factor is defined as the ratio of total force normal to the surface, normalized with respect to the thrust of the secondary jet,

$$A \equiv \frac{F_i + F_j}{F_j} \tag{12}$$

then the amplification factor is a constant for high pressure ratios and a given set of primary conditions.

Dahm [Ref. 9] developed an expression for side force based on second order blast wave theory

$$F_i = P_\infty A_* \left(\frac{16\, \omega_2^{\frac{3}{2}} M_\infty K_1^2}{\pi^2 J_0^{\frac{3}{2}}} \right)^{\frac{1}{2}} \left(\frac{s}{d_*} \right)^{\frac{1}{2}} \left(\frac{\dot{m}_s V_\infty}{P_\infty A_*} \right)^{\frac{3}{4}} \tag{13}$$

where

$$\omega_2 = \frac{1}{2} + \frac{1}{\gamma_p(\gamma_p-1)M_\infty^2} + \left(\frac{\gamma_s}{\gamma_s-1}\right)\left(\frac{1+\frac{\gamma_p-1}{2}M_\infty^2}{\gamma_p M_\infty^2}\right)\frac{m_p T_{ST}}{m_s T_{PT}}$$

Dahm states that the characteristic blast wave radius R_o is described by

$$R_o = \left(\frac{\omega_2 \dot{m}_s V_\infty}{.2\pi P_\infty}\right)^{\frac{1}{2}} \tag{14}$$

Solving ω_2 from Equation (14) and substituting into Equation (13) it can be shown that since

$$F_i \propto \omega_2^{\frac{3}{4}} \tag{15}$$

and

$$\omega_2 \propto R_o^2 \tag{16}$$

then

$$F_i \propto R_o^{\frac{3}{2}} \tag{17}$$

After comparing the values for side force given by Equation (13) with experimental results, Dahm suggested that the equation be multiplied by 0.51 to yield a semi-empirical equation that more closely correlates with experimental results. Dahm noted considerable scattering of the data at low secondary injection flow rates and suggested that these values were outside the range of validity of his theory.

V. EXPERIMENTAL RESULTS

The results of these experiments were obtained for a single set of primary flow conditions. The primary Mach number was 1.92 ± 0.01, the primary total pressure was held at 30 psi, and the primary total temperature was $510^{o}R \pm 15^{o}$. Other data were obtained by measuring the separation distance from photographs used by Chrans and Collins at Mach number 2.80 and a primary total pressure of 50 psi.

The injectant pressure was varied from 20 psi to 180 psi to obtain pressure ratios from 2/3 to 6. Injectant temperature was varied from $500^{o}R$ to $1200^{o}R$ to obtain temperature ratios of from 1 to 2.4. Nitrogen, argon and helium were used as injectant gases to provide a substantial range of molecular weight effects. The sonic nozzle exit diameter was also varied.

In this experiment the discharge coefficient of the sonic nozzle was found by dividing the actual mass flow rate through the nozzle by the corresponding mass flow rate calculated for ideal gas assuming isentropic flow. The actual flow rate was measured with the use of a sharp-edged orifice flowmeter located in the injectant supply line. Figure 10 is a plot of discharge coefficient versus the inverse square root of nozzle exit Reynolds number. These results are in agreement with the discharge coefficients calculated for the same nozzle in Ref. 1.

A. PENETRATION HEIGHT

The penetration height of the injectant was scaled from the Schlieren photographs which were made of each run. The depth of

penetration was taken as the maximum height reached by the under-expanded jet above the surface of the tunnel floor. This distance was easily determined for all runs using nitrogen or argon as the injectant. When helium was used as the injectant, lack of definition in the photographs limited determination of penetration height to a few runs using the larger injection nozzle.

Figure 11 is a plot of the non-dimensional penetration height as a function of the ratio of secondary to primary total pressure. Good agreement is obtain both with the theory of Zukoski and Spaid and with the theory of Cassel, Davis and Engh, with the latter more closely correlating with the experimental data. A mean curve scaled from the experimental data of Koch is plotted for comparison. It appears that for the lower primary Mach number and pressure (M_∞ =1.92, P_{pt}=30 versus M_∞= 2.8, P_{pt}=50) slightly better agreement is obtained with both Zukoski and Spaid theory and Cassel, Davis and Engh theory.

Although the stagnation temperature ratio was varied up to a factor of 2.4 while holding the secondary stagnation pressure constant, no essential difference in the penetration height could be detected. This is in agreement with the observation of Chrans and Collins. Within the limit of data scatter the penetration height does not appear to be a function of molecular weight.

B. SIDE FORCE

In Figs. 12 and 13 interaction side force is plotted against the blast wave characteristic radius and the penetration height, respectively, for comparison with theory. Zukoski and Spaid derived the relationship

$$F_i \propto h^2 \qquad (8)$$

and Dahm derived the relationship

$$F_i \propto R_o^{\frac{3}{2}} \tag{17}$$

In Fig. 12 it is shown that the Dahm theory is in reasonable agreement with the data at the higher values of R_o; however, the function

$$F_i \propto R_o \tag{18}$$

appears to more closely describe the general trend of the experimental data.

In Fig. 13 the data is more scattered than in Fig. 12 since h is a measured quantity as opposed to R_o which is a calculated quantity. Since Chrans and Collins determined that a unique relationship exists between h and R_o, it would appear that an exponent of unity, rather than the value 2 predicted by Zukoski and Spaid, would more closely describe the trend of this data also.

C. SEPARATION DISTANCE

Separation distance was taken as the distance from the center of the injection point upstream to the intersection of the separation shock and the floor of the tunnel. This distance is non-dimensionalized with respect to the penetration height and plotted in Figs. 14 and 15 versus total pressure ratio multiplied by effective nozzle diameter. This pressure ratio, with correction, can be considered non-dimensionalized with respect to some tunnel dimension here taken as unity for convenience.

Figure 14 is a plot of data taken from photographs used by Chrans and Collins at Mach number 2.80. An unscaled curve representing the data of Fig. 14 is plotted on Fig. 15 for comparison with data for Mach number 1.92. The values predicted by the theory of Wu, Chapkis and Mager show good agreement with experimental values although the data do not appear to be dependent on the Mach number or the ratio of specific heats, as predicted by Wu, Chapkis and Mager theory.

A physical interpretation of the parameter $\frac{\Delta x}{h}$ is given by Wu, Chapkis and Mager as

$$\frac{\Delta x}{h} = \cot \theta \tag{19}$$

where θ is the separation angle. An examination of Schlieren photographs, however, indicates that arccot $\frac{\Delta x}{h}$ is not physically the same as the separation angle and indeed may sometimes be larger and sometimes be smaller than the separation angle, depending upon the distance between the nozzle centerline and the induced bow shock. The physical difference between arccot $\frac{\Delta x}{h}$ and θ may account for the difference in trend between theory and experimental data.

A plot of separation distance versus secondary momentum flux is shown in Fig. 16. Data correlation is noticeably better than that observed in Fig. 15.

D. AMPLIFICATION FACTOR

The side force amplification factor is plotted against secondary momentum flux in Fig. 17, and total pressure ratio corrected for nozzle diameter is shown in Fig. 18. A curve representing the data of Koch for Mach 2.80 is presented for comparison in both figures, along

with the semi-empirical curve of Dahm. From Figs. 17 and 18 it can be observed that the amplification factor decreases with increasing stagnation pressure ratio and increasing momentum flux. In each plot the amplification factor appears to be asymptotically approaching a value in the range 1.5 to 2.0. This approach to a constant amplification factor at high pressure ratios agrees qualitatively with the theory of Zukoski and Spaid. Considerable scatter in the data can be observed in the area of low injection pressures. At the higher injection pressure ratios, the scatter is reduced and better agreement is obtained with the theory of Dahm and with the data of Koch. There appears to be no systematic dependence on primary Mach number.

Figure 19 is a plot of amplification factor versus secondary mass flow rate, and Fig. 20 is a plot of amplification factor versus secondary stagnation temperature. Experimental runs represented by these data were conducted at a constant secondary stagnation pressure of 120 psi with secondary stagnation temperatures from 510°R to 1200°R. Although molecular weight variations introduce some variation in momentum flux, the difference is not considered significant and the data may be considered to be for constant momentum flux as well as constant injection pressure. Figures 19 and 20 indicate that no essential difference in amplification factor is obtained by heating of the injectant gas and, since amplification factor remains essentially constant for different mass flow rates at constant injection pressure, the amplification factor does not appear to be mass dependent.

Figure 21 is a cross-plot of amplification factor and separation distance non-dimensionalized with respect to penetration height.

The amplification factor increases with increasing $\frac{\Delta x}{h}$ and may be empirically described by

$$A = 0.65 \left(\frac{\Delta x}{h}\right)^{1.5} \tag{20}$$

Good correlation of the data with this empirical equation is indicated for all injectant gases, all injectant stagnation temperatures and both nozzle diameters.

VI. CONCLUSIONS

Penetration height increases with increasing total pressure ratio and is well predicted by the theory of Zukoski and Spaid and the theory of Cassel, Davis and Engh. At Mach number 1.92 the theory of Cassel, Davis and Engh is in better agreement with experimental data than the theory of Zukoski and Spaid. The significance of primary Mach number and pressure as scaling parameters of penetration height appears to be correctly given by the theory of Zukoski and Spaid. The penetration height is not a function of injectant stagnation temperature, or is at most a weak function of that temperature.

The trend in the amplification factor toward a constant value at high pressure ratios supports the theory of Zukoski and Spaid. Also at high pressure ratios the experimental values of amplification factor are well predicted by the theory of Dahm, although for low injection pressure ratios there is considerable variation between theory and experimental data.

Separation distance non-dimensionalized with respect to penetration height decreases with pressure ratio and secondary momentum flux in the same manner as does the side force amplification factor. Since it has been shown by several investigators that the area upstream of the injection nozzle is subjected to the greatest increase in pressure due to interaction, a close relationship between the separation distance and the amplification factor is not unexpected. The correlation between these two parameters is empirically given by

$$A = 0.65 \left(\frac{\Delta x}{h}\right)^{1.5} \qquad (20)$$

which is shown by the data to be independent of, or at most a weak function of, injection stagnation temperature.

For constant injection stagnation pressure the amplification factor is essentially independent of injection stagnation temperature and secondary mass flow rate. The data tend to support the conclusion that the side force amplification factor is a function of secondary momentum flux.

Within the scatter of the data experimental results indicate that, for constant secondary momentum, the side force amplification does not vary with changes in molecular weight of the secondary gas.

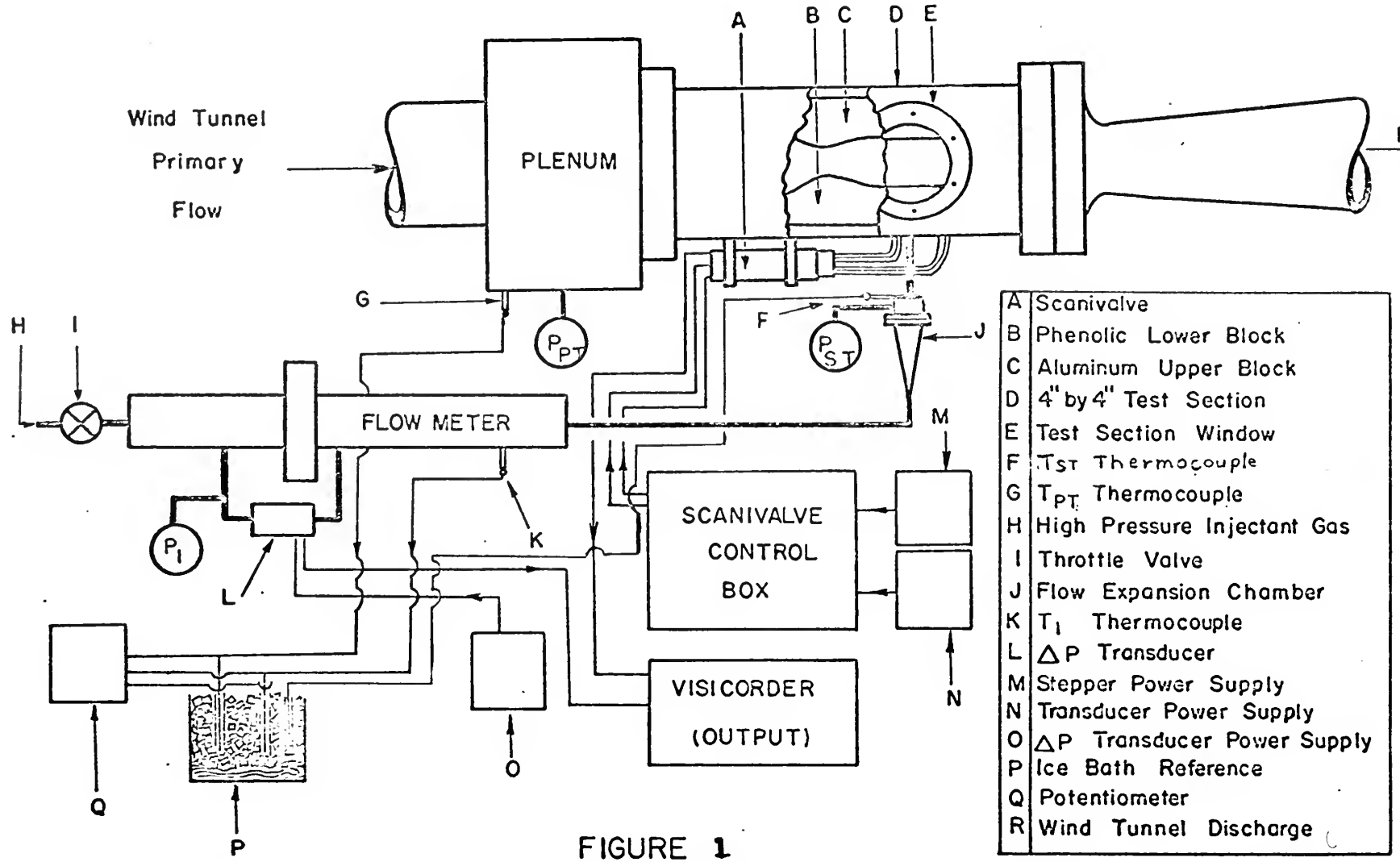

FIGURE 1
EQUIPTMENT SCHEMATIC

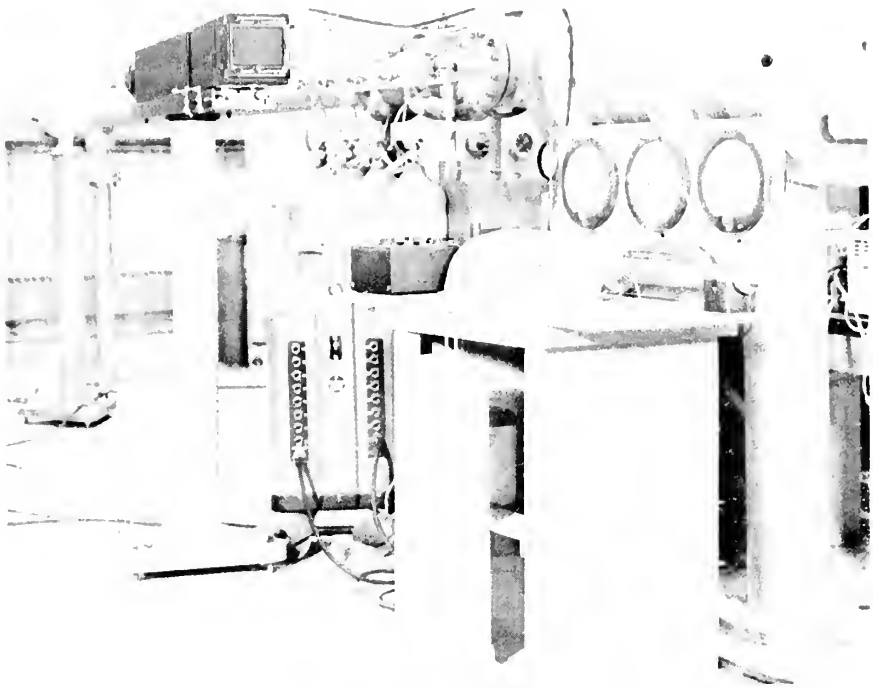

FIGURE 2
PHOTOGRAPH OF TEST SETUP

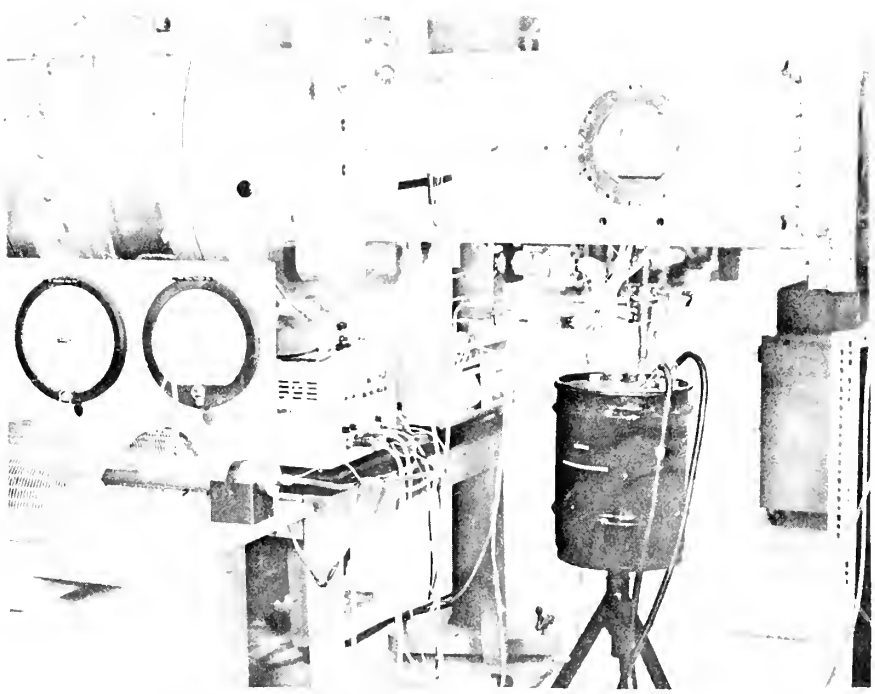

FIGURE 3
PHOTOGRAPH OF TEST SETUP

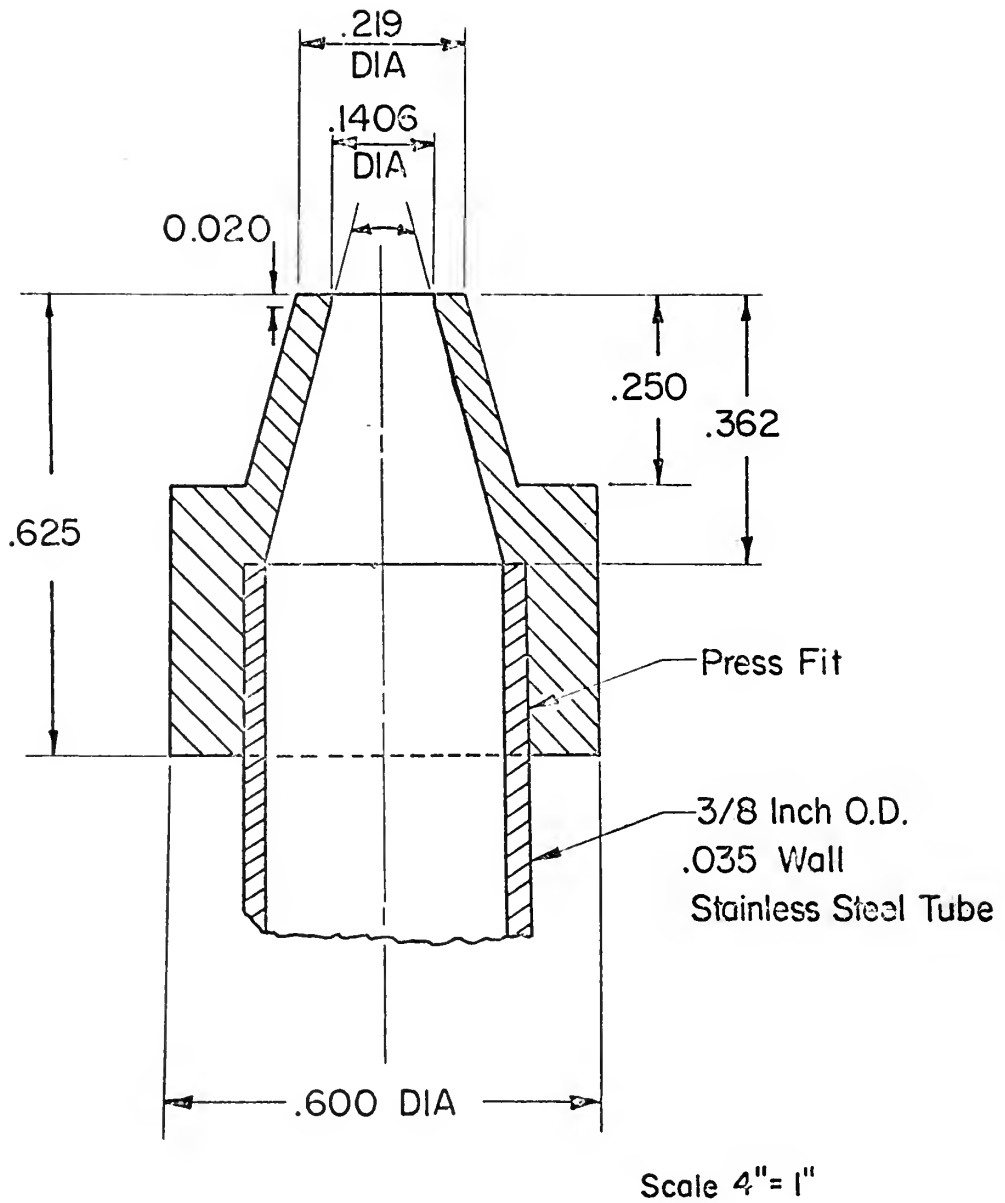

FIGURE 4. SONIC NOZZLE DIAGRAM

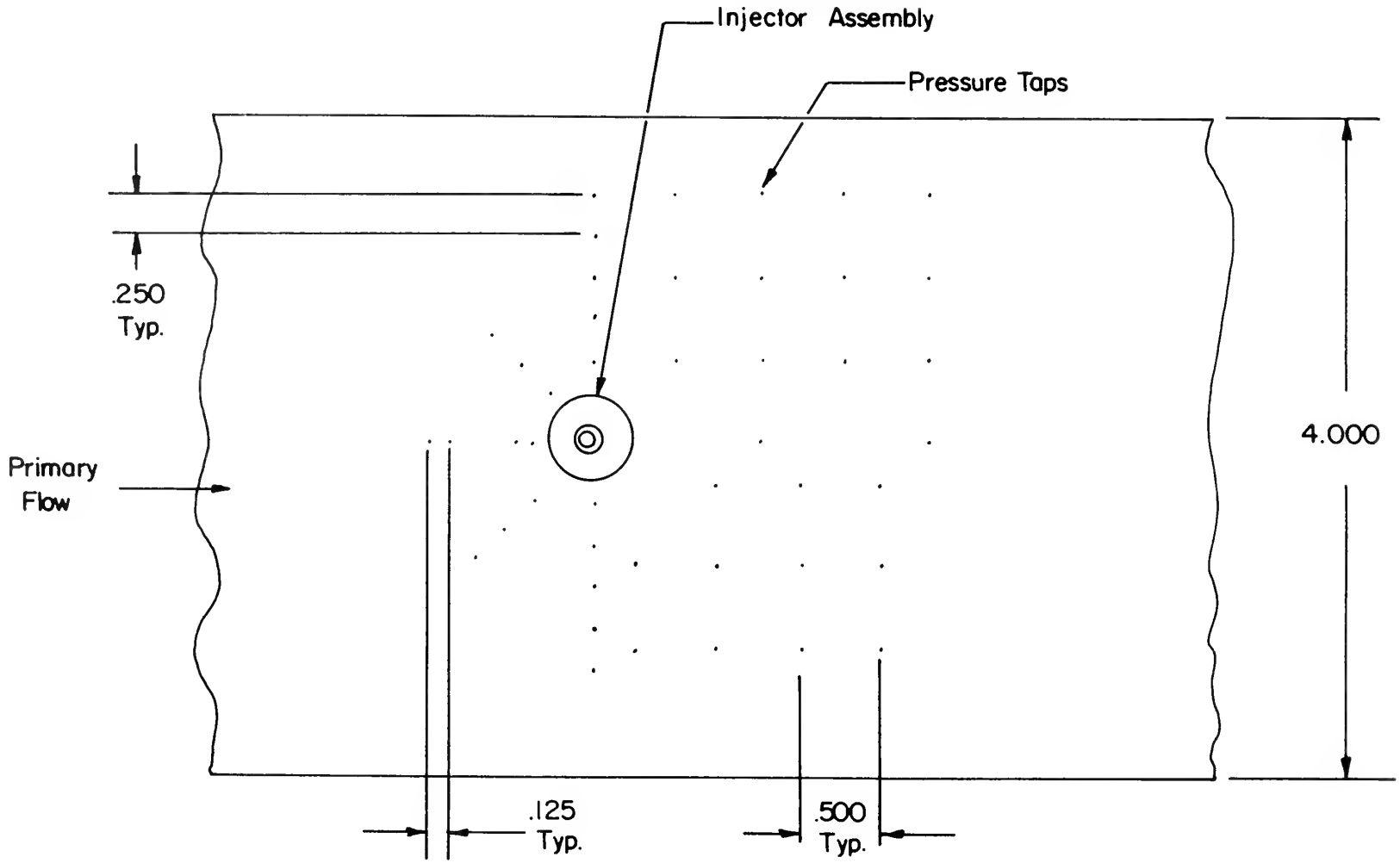

FIGURE 5
TOP VIEW OF TEST SECTION

		d = 0.1406				d=0.075
Injectant	P_{ST} \ T_{ST}	500°	700°	1000°	1200°	500°
NITROGEN	20	1				
	30	2				56
	60	3				57
	120	4	37	38	39	58
	150	5				59
	180	6				60
HELIUM	60	8				
	90	9				
	120	10	43	44	45*	
	150	11				
	180					66
ARGON	20	13				
	30	14				
	60	15				
	120	16	40	41	42	
	150					71

* RUN #45 T_{ST} = 1030°

FIGURE 6.
EXPERIMENTAL RUN MATRIX

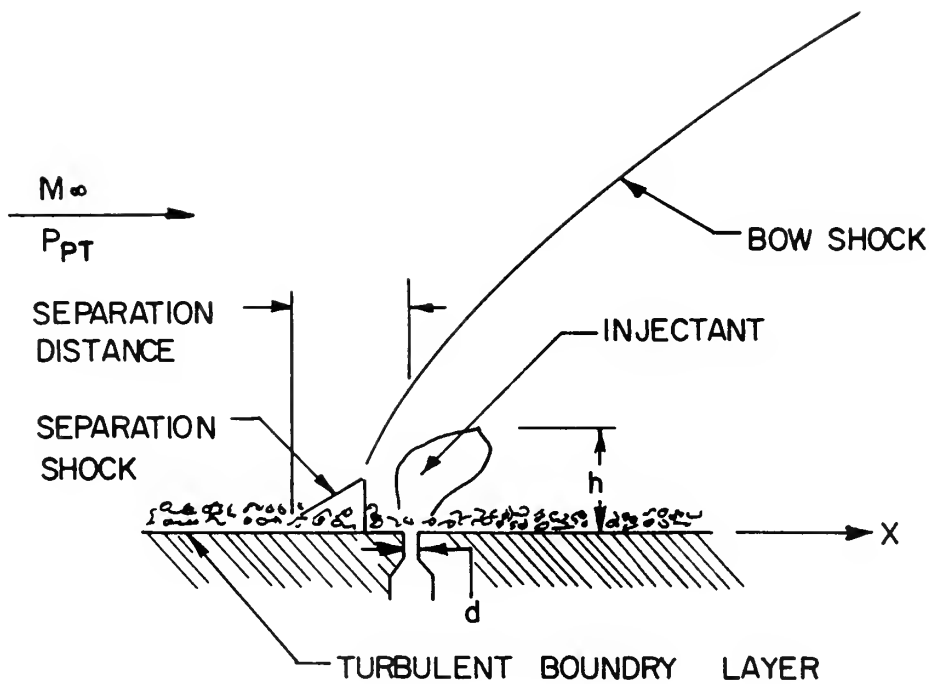

FIGURE 7. FLOW FIELD SKETCH

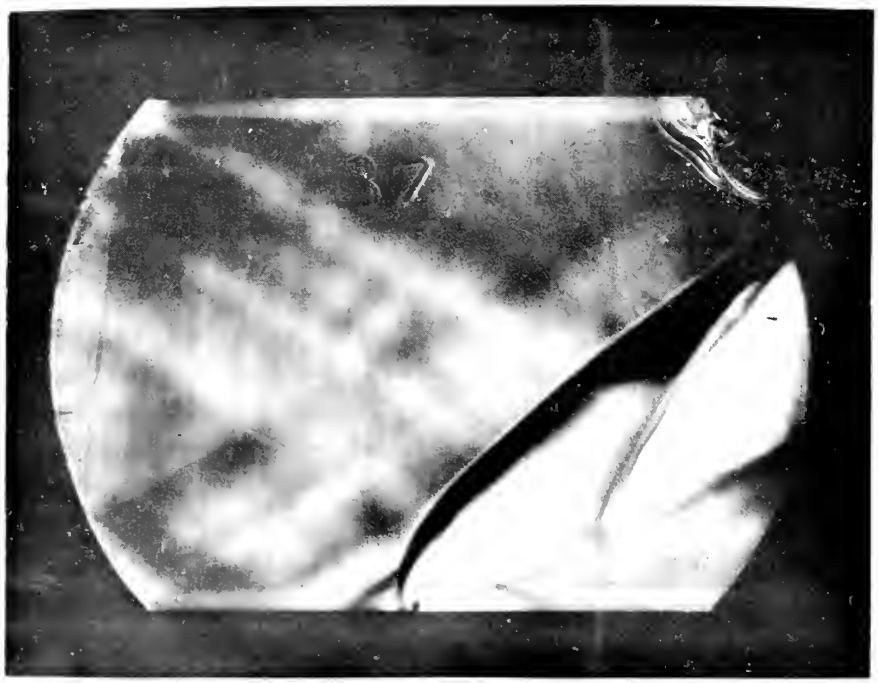

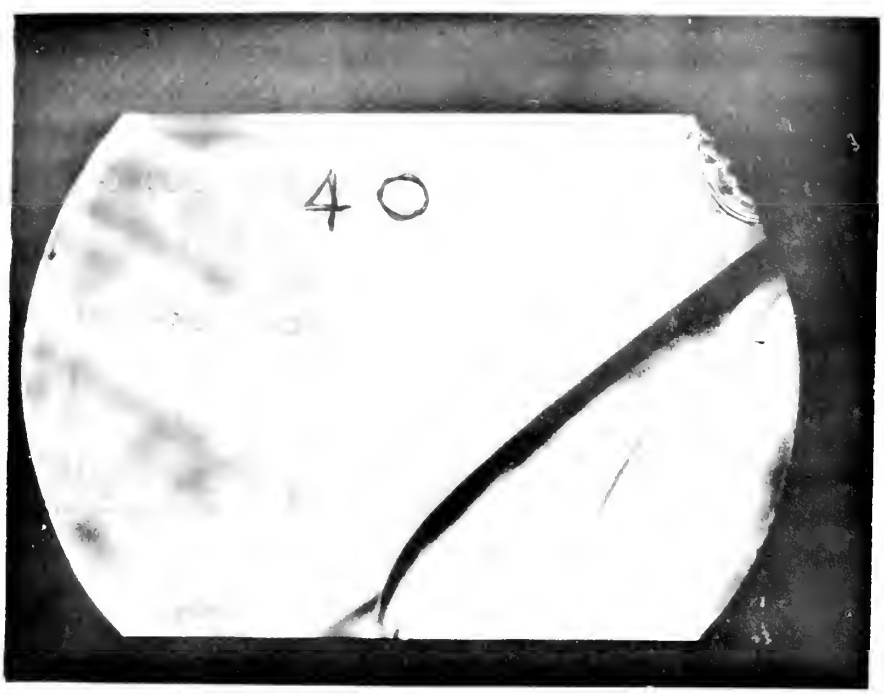

PLATE 9

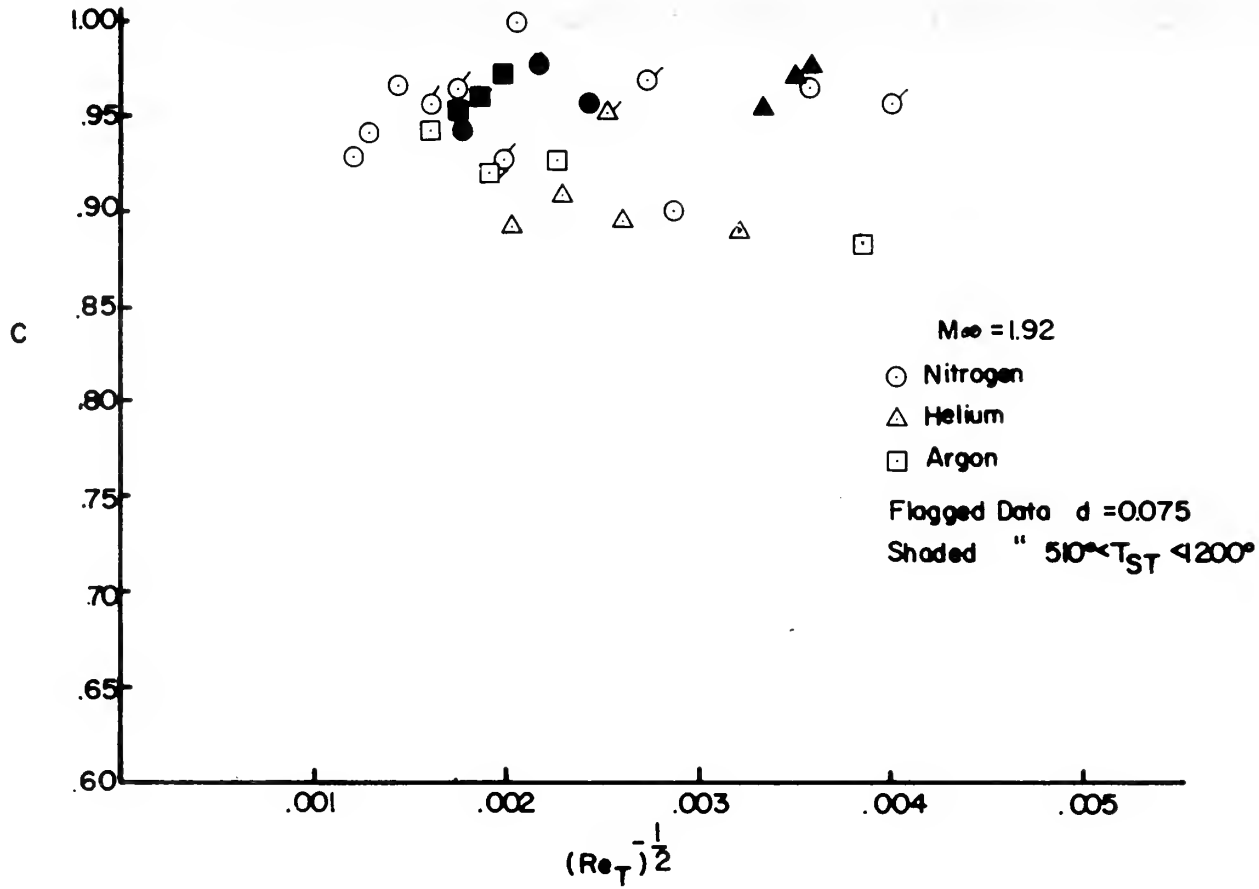

FIGURE 10

NOZZLE DISCHARGE COEFFICIENT VS. INVERSE SQUARE ROOT OF Re_T

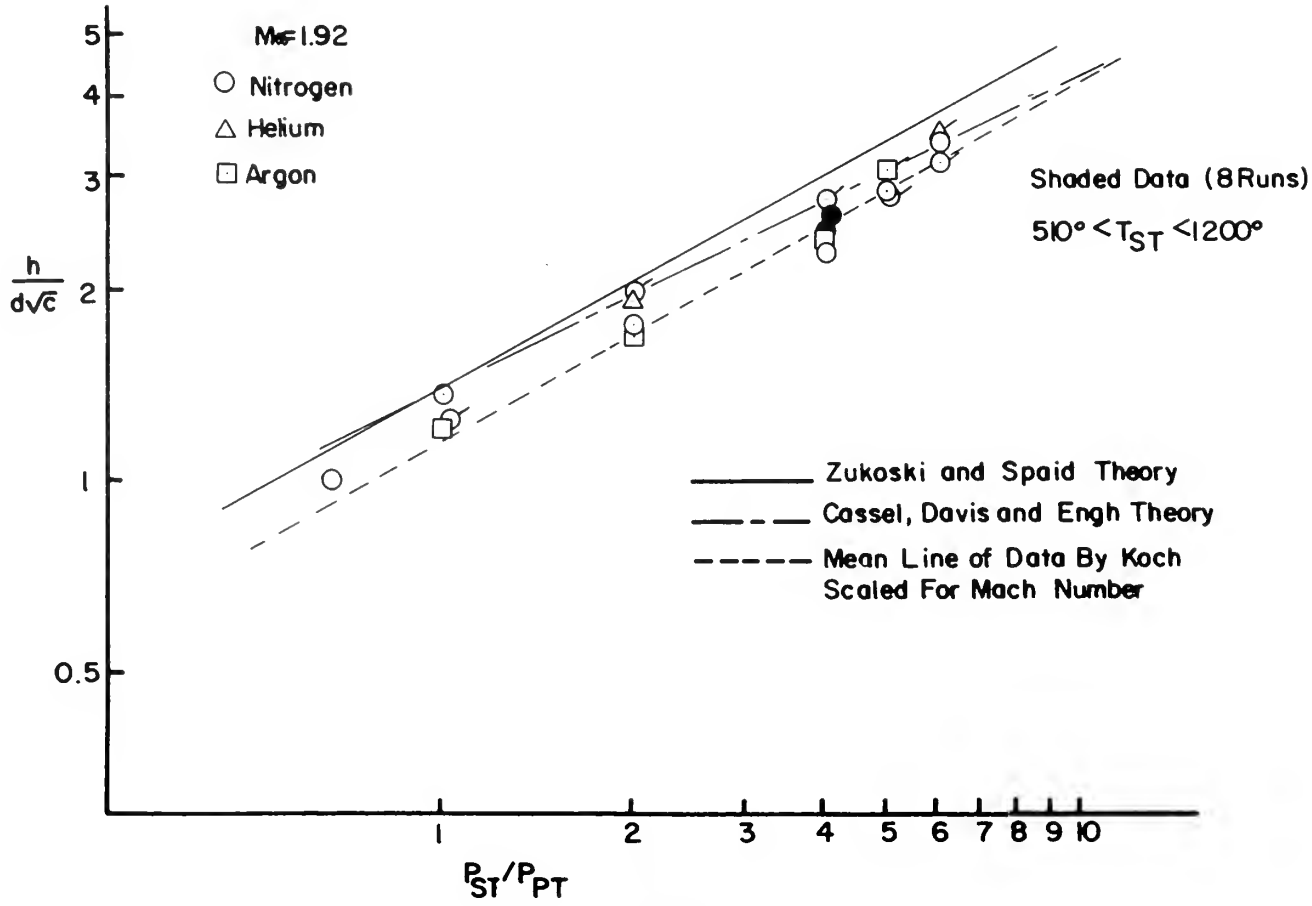

FIGURE 11

NON-DIMENSIONAL PENETRATION HEIGHT VS. TOTAL PRESSURE RATIO

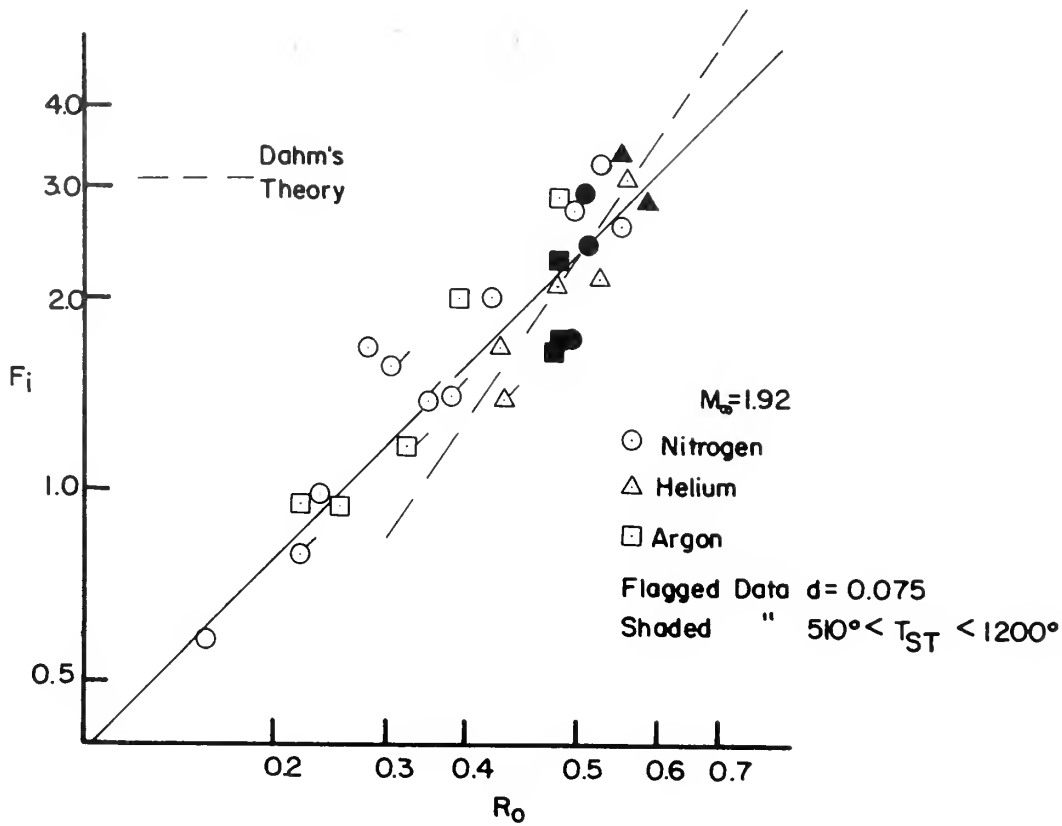

FIGURE 12

INTERACTION SIDE FORCE VS. BLAST WAVE CHARACTERISTIC RADIUS.

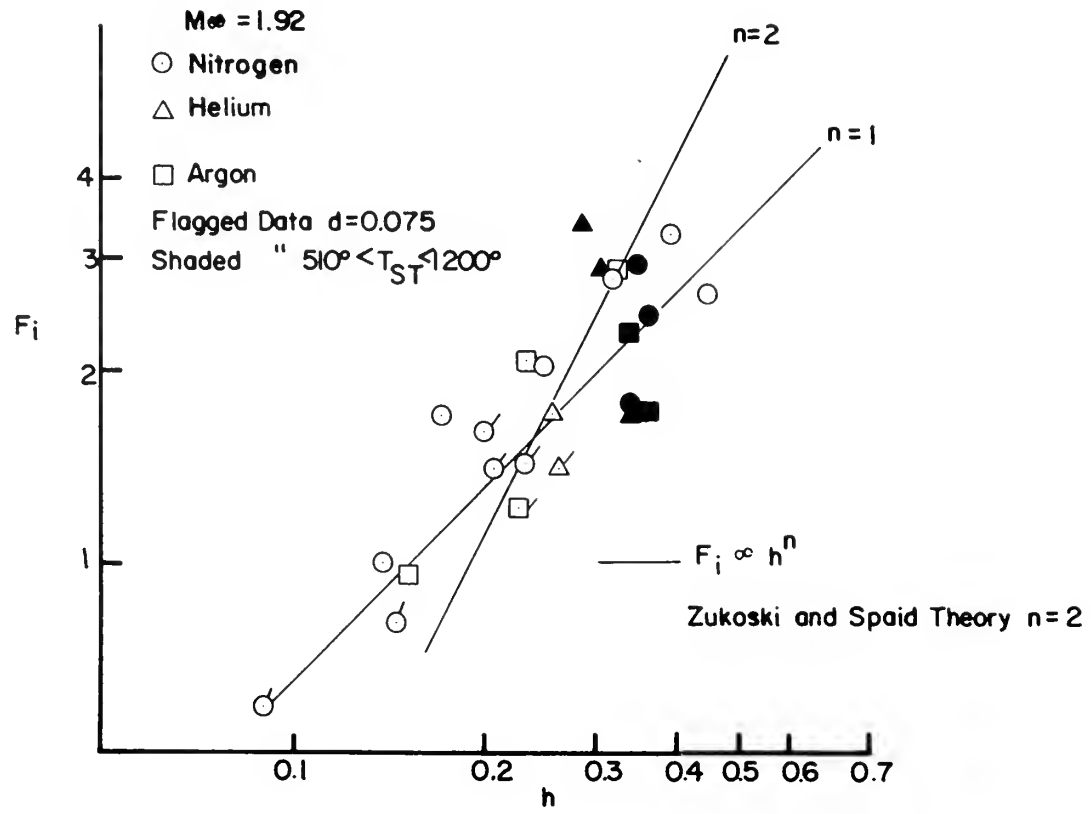

FIGURE 13

SIDE FORCE VS. PENETRATION HEIGHT

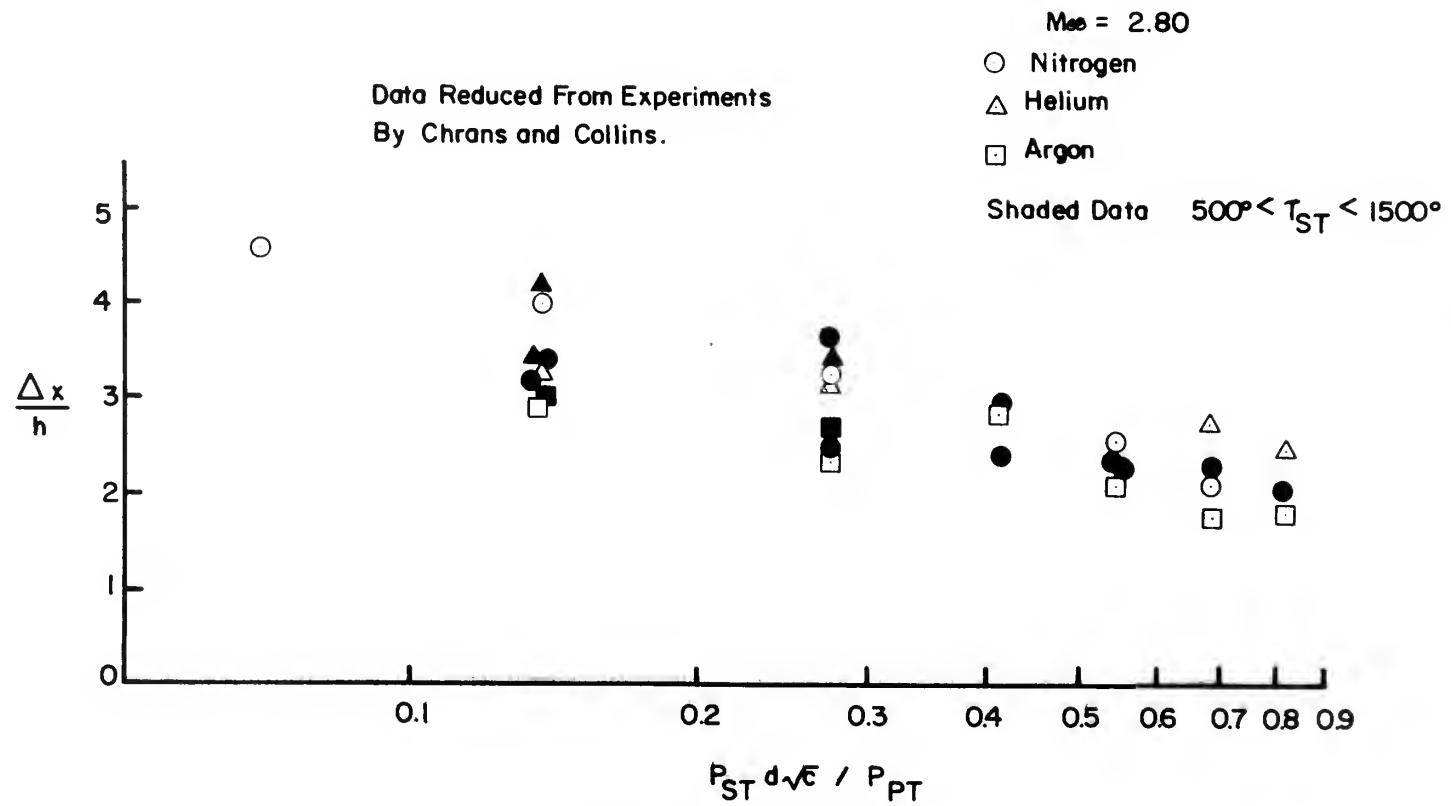

FIGURE 14

$\frac{\Delta x}{h}$ VS. TOTAL PRESSURE RATIO CORRECTED FOR NOZZLE DIAMETER.

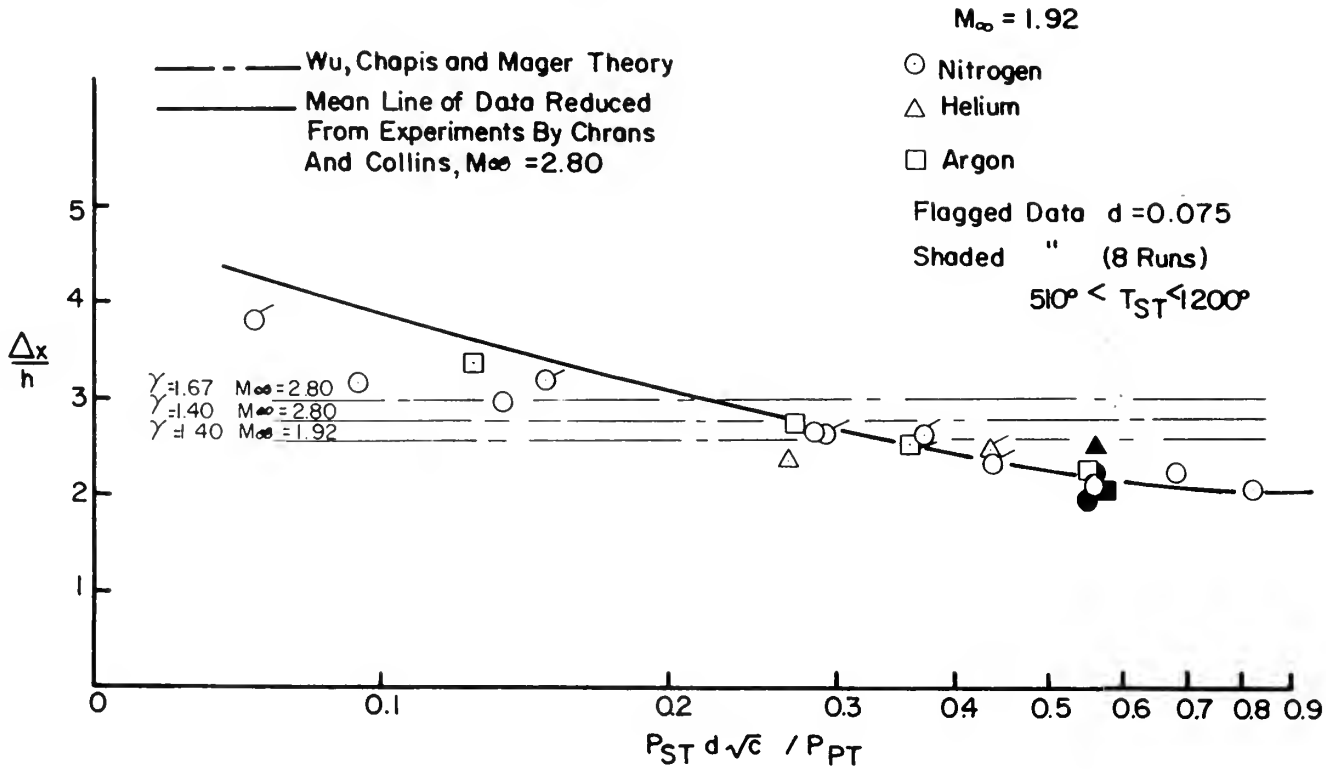

FIGURE 15

$\frac{\Delta x}{h}$ VS. TOTAL PRESSURE RATIO CORRECTED FOR NOZZLE DIAMETER

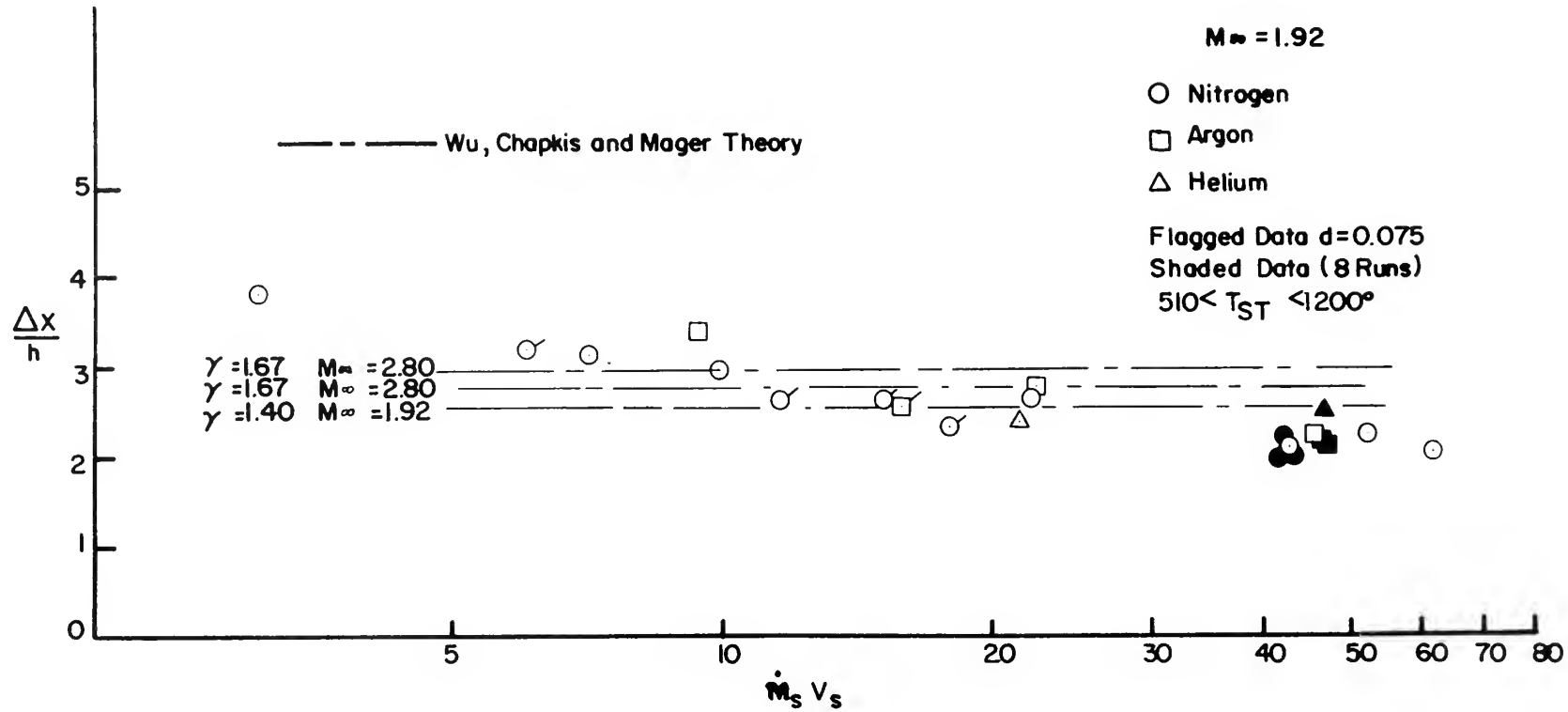

FIGURE 16

$\frac{\Delta x}{h}$ VS. SECONDARY MOMENTUM FLUX

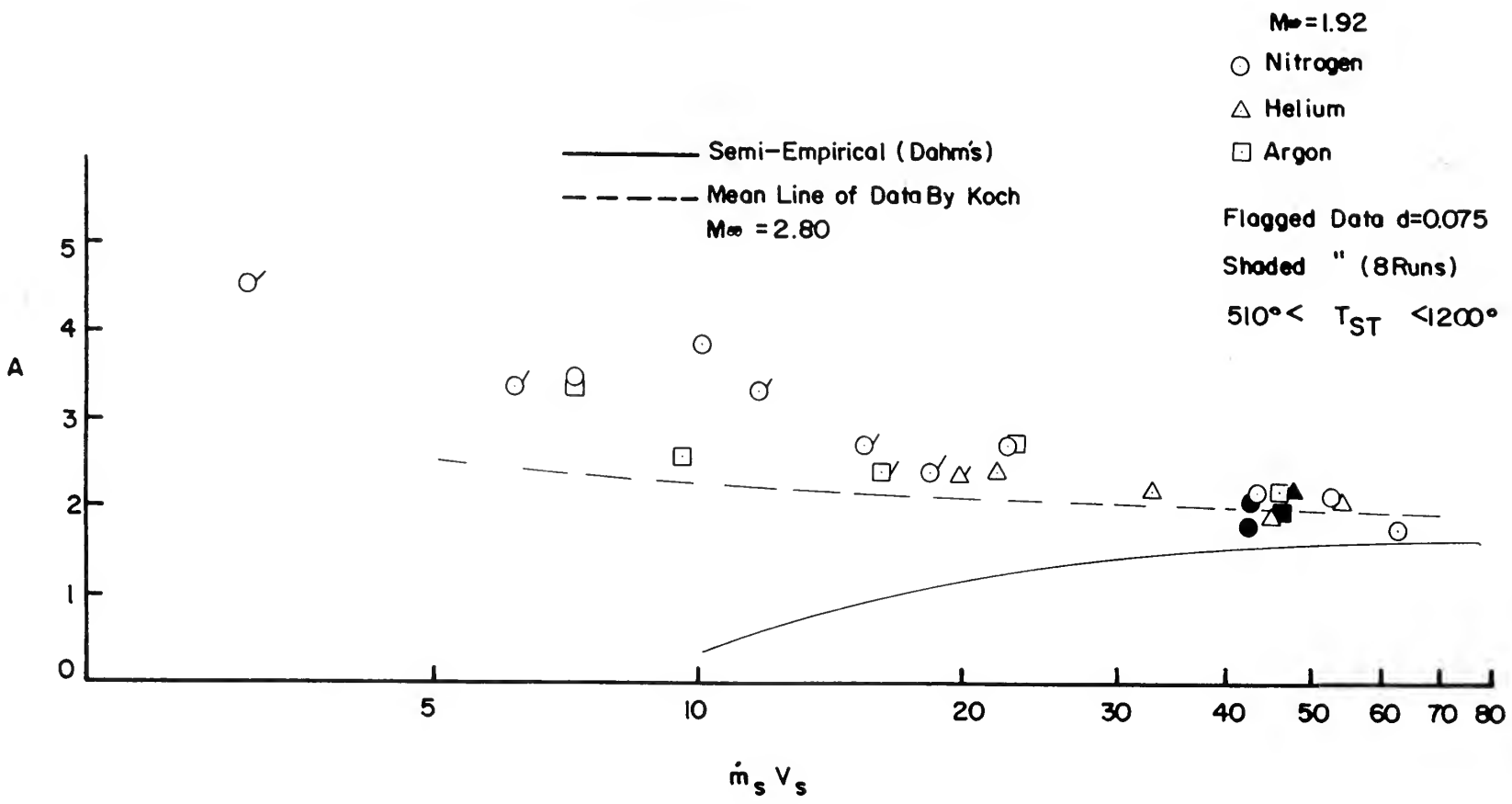

FIGURE 17

FORCE AMPLIFICATION FACTOR VS. SECONDARY MOMENTUM FLUX.

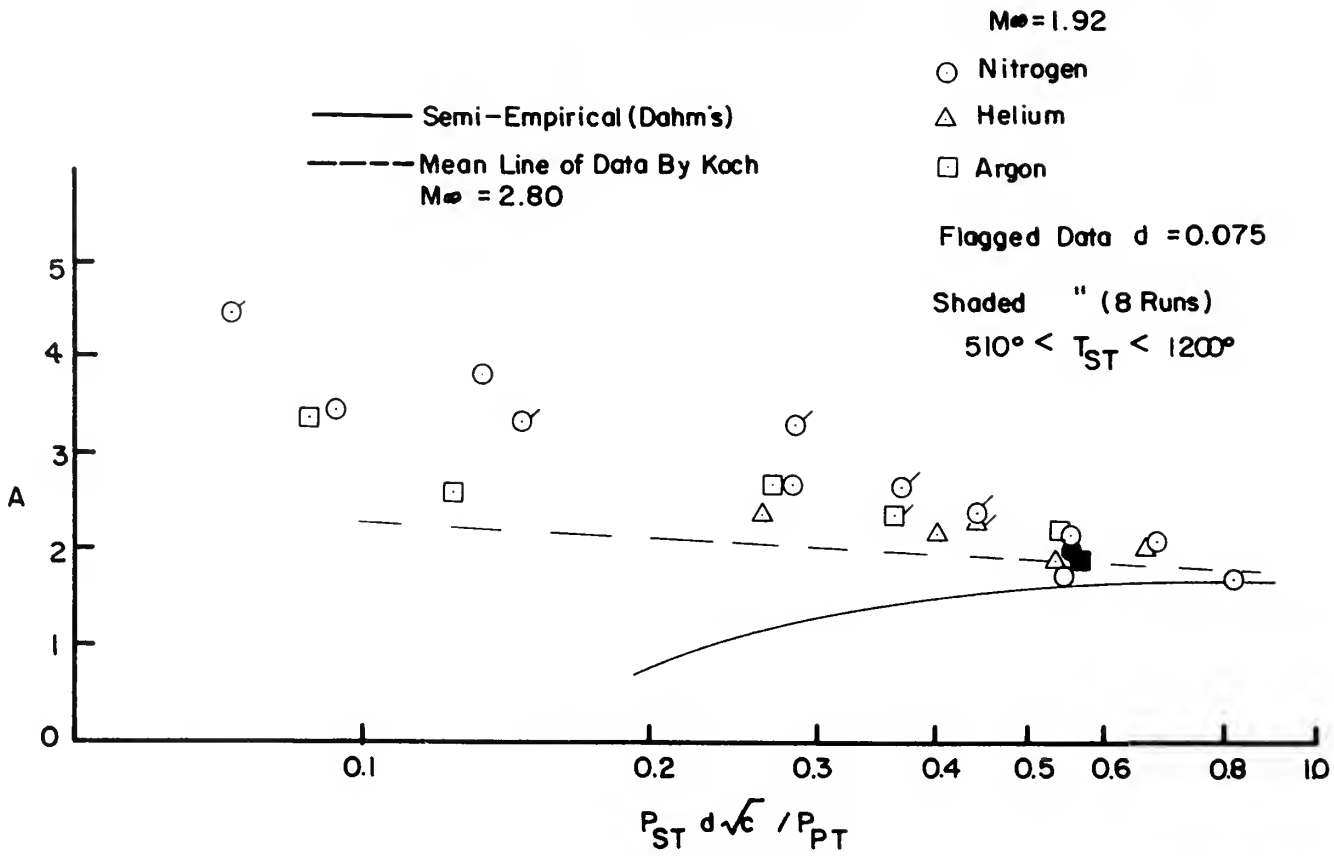

FIGURE 18

FORCE AMPLIFICATION FACTOR VS. TOTAL PRESSURE RATIO CORRECTED FOR NOZZLE DIAMETER.

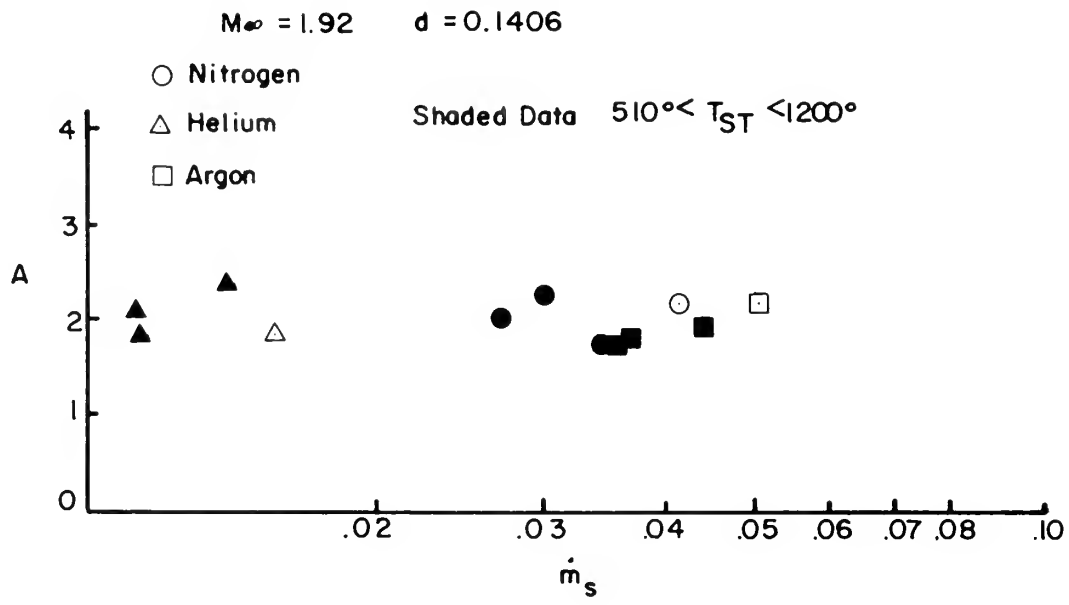

FIGURE 19

FORCE AMPLIFICATION FACTOR VS. SECONDARY MASS FLOW RATE

(P_{ST} =120)

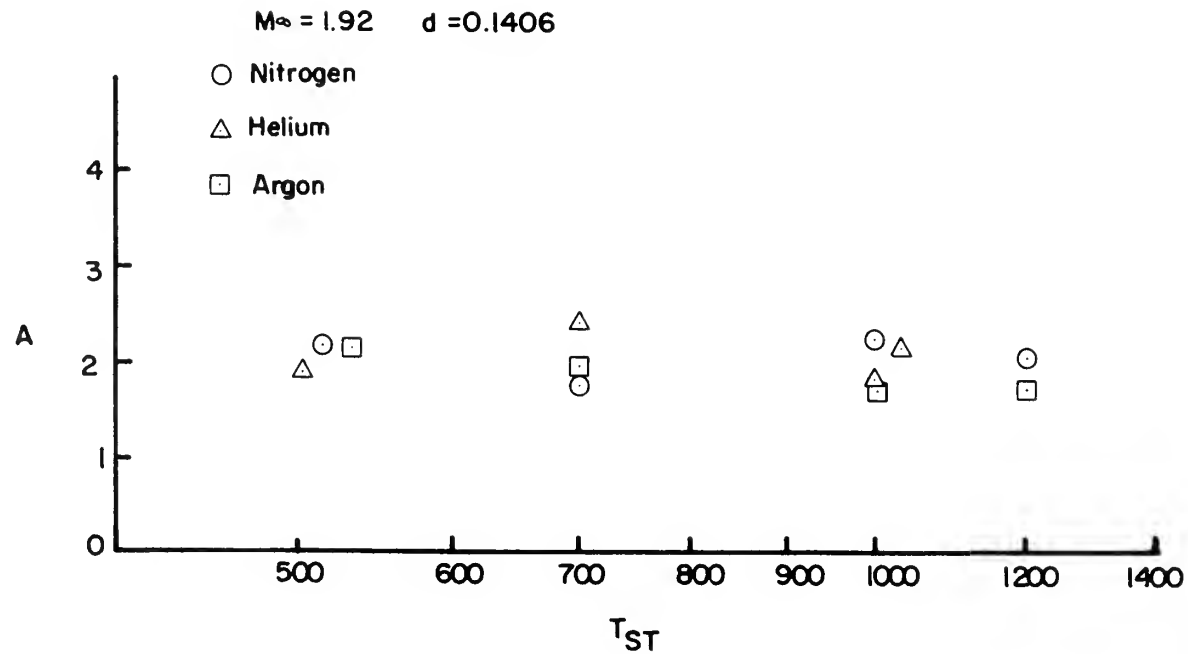

FIGURE 20

FORCE AMPLIFICATION FACTOR VS. SECONDARY TOTAL TEMPERATURE (P_{ST}= 120).

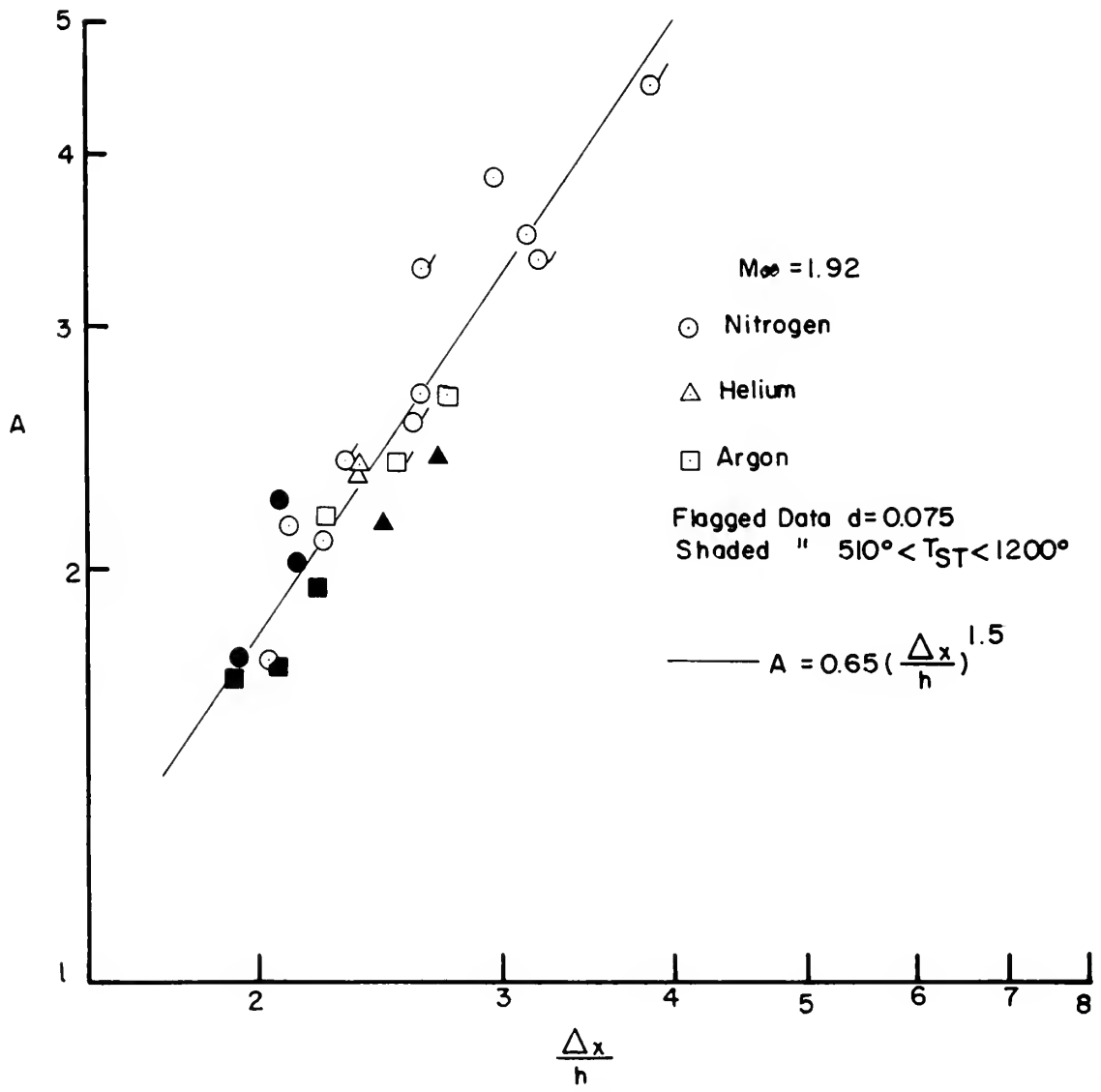

FIGURE 21

SIDE FORCE AMPLIFICATION FACTOR VS. $\frac{\Delta x}{h}$

LIST OF REFERENCES

1. AIAA Paper No. 69-1, The Effect of Stagnation Temperature and Molecular Weight Variation of Gaseous Injection into a Supersonic Stream, by L. J. Chrans and D. J. Collins, January 1969.

2. Liepmann, H. W. and Roshko, A., Elements of Gas Dynamics, John Wiley and Sons, Inc., 1957.

3. Zukoski, E. E., and Spaid, F. W., "Secondary Injection of Gases into a Supersonic Flow," AIAA Journal, 2, p. 1689-1696, October 1964.

4. Koch, L. N., The Effect of Varying Secondary Mach Number and Injection Angle on Secondary Gaseous Injection into a Supersonic Flow, A. E. Thesis, U. S. Naval Postgraduate School, Monterey, California, 1969.

5. U. S. Army Missile Command Report No. RD-TR-68-5, Lateral Jet Control Effectiveness Prediction for Axisymmetric Missile Configurations, by L. A. Cassel, J. G. Davis and D. P. Engh, June 1968.

6. NACA Report 1135, Equations, Tables and Charts for Charts for Compressible Flow, by Ames Research Staff, 1953.

7. Wu, J. M., Chapkis, R. E., and Mager, A., "Approximate Analysis of Thrust Vector Control by Fluid Injection," American Rocket Society Journal, p. 1677-1685, December 1961.

8. Hammitt, A. G., and Murthy, K. R. A., "approximate Solutions for Supersonic Flow over Wedges and Cones," AFOSR TN 59-304, Rep 449, Princeton Univ., April 1959.

9. Vidya Technical Note No. 9166-TN-3, The Development of an Analogy to Blast Wave Theory for the Prediction of Interaction Forces Associated with Gaseous Secondary Injection into a Supersonic, by T. J. Dahm, May 1964.

INITIAL DISTRIBUTION LIST

		No. Copies
1.	Defense Documentation Center Cameron Station Alexandria, Virginia 22314	20
2.	Library Naval Postgraduate School Monterey, California 93940	2
3.	Professor D. J. Collins Department of Aeronautics Naval Postgraduate School Monterey, California 93940	1
4.	Chairman, Department of Aeronautics Naval Postgraduate School Monterey, California 93940	1
5.	Commander Naval Air Systems Command Headquarters Washington, D. C. 20360 AIR-03C (1) AIR-310 (1) AIR-320 (1) AIR-330B (1) AIR-536 (1) AIR-5366 (1) AIR-5367 (1) AIR-538 (1) AIR-303 (1)	9
6.	Commander Naval Ordnance Systems Command Headquarters Washington, D. C. 20360 ORD-03B (1) ORD-033 (1)	2
7.	Chief of Naval Research Dr. Ralph Roberts (Code 429) Navy Department Washington, D. C. 20360	1

8. Naval Ordnance Station — 1
Dr. G. Testi (Code RR)
Indian Head, Maryland 20640

9. Army Missile Command — 2
Research and Development Directorate
Redstone Arsenal
Huntsville, Alabama 35809

Propulsion Laboratory, F. James (1)
Library (1)

10. Commander — 4
Naval Weapons Center
China Lake, California 93555

Code 608 (1)
Code 451 (1)
Code 458 (1)
Library (1)

11. Commander — 2
Naval Ordnance Laboratory
White Oak
Silver Spring, Maryland 20910

Code 310 (1)
Library (1)

12. Commanding Officer and Director — 2
Naval Ships Research and Development Center
Washington, D. C. 20007

Code 600 (1)
Library (1)

13. Applied Physics Laboratory — 1
8621 Georgia Avenue
Silver Springs, Maryland 20910

14. Air Force Aero-Propulsion Laboratory — 2
Wright-Patterson Air Force Base, Ohio 45433

APG (1)
APX (1)

15. Air Force Armament Laboratory — 2
Eglin Air Force Base, Florida 32544

ATW (1)
ATZ (1)

16. Air Force Rocket Propulsion Laboratory — 7
Edwards Air Force Base, California 93523

RPM (1)
RPMC (1)
RPPP (1)
RPR (1)
RPRE (1)
RPRP (1)
RPX (1)

17. Air Force Flight Dynamics Laboratory — 1
Wright-Patterson Air Force Base, Ohio 45433

18. CO, Navy Space Systems Activity — 1
Hq. Air Force Space Systems Division
Air Force Unit Post Office
Los Angeles, California 90045

19. Commandant of the Marine Corps (Code A03C) — 1
Headquarters, U. S. Marine Corps
Washington, D. C. 20380

20. James Carson Breckinridge Library — 1
Marine Corps Development and Educational Command
Quantico, Virginia 22134

21. Captain Russel A. Chambers — 1
3028 Hiawatha
Kansas City, Kansas 66104

Security Classification

DOCUMENT CONTROL DATA - R & D

(Security classification of title, body of abstract and indexing annotation must be entered when the overall report is classified)

1. ORIGINATING ACTIVITY (Corporate author)	2a. REPORT SECURITY CLASSIFICATION
Naval Postgraduate School Monterey, California 93940	Unclassified
	2b. GROUP

3. REPORT TITLE

The Effect of Varying Secondary Stagnation Temperature and Molecular Weight on the Side Force Generated by Gaseous Injection into a Supersonic Stream

4. DESCRIPTIVE NOTES (Type of report and inclusive dates)

Master's Thesis; October 1969

5. AUTHOR(S) (First name, middle initial, last name)

Russel Allen Chambers

6. REPORT DATE	7a. TOTAL NO. OF PAGES	7b. NO. OF REFS
October 1969	51	9

8a. CONTRACT OR GRANT NO.	9a. ORIGINATOR'S REPORT NUMBER(S)
b. PROJECT NO.	
c.	9b. OTHER REPORT NO(S) (Any other numbers that may be assigned this report)
d.	

10. DISTRIBUTION STATEMENT

This document has been approved for public release and sale; its distribution is unlimited.

11. SUPPLEMENTARY NOTES	12. SPONSORING MILITARY ACTIVITY
	Naval Postgraduate School Monterey, California 93940

13. ABSTRACT

This study was undertaken to investigate the effects of varying the injectant temperature and molecular weight on the flow field generated by the interaction of a secondary jet with a supersonic mainstream. The experimental portions of this investigation were conducted at a primary Mach number of 1.92 in the Naval Postgraduate School Supersonic Wind Tunnel. Data are presented and compared with theory. This presentation includes correlation of the penetration height of the secondary flow, interaction side force amplification factor, and separation distance non-dimensionalized with respect to the penetration height.

DD FORM 1 NOV 65 1473 (PAGE 1)

S/N 0101-807-6811

Security Classification

A-31408

14 KEY WORDS	LINK A		LINK B		LINK C	
	ROLE	WT	ROLE	WT	ROLE	WT
Supersonic						
Interaction						
Side force						
Injection						
Secondary jet						
Heating						